Effect of process parameters on grain structure formation during VAR of INCONEL alloy 718

A. KERMANPUR*
Department of Materials, Imperial College London, London SW7 2BP, UK

D. G. EVANS
Special Metals Corporation, New Hartford, NY 13413, USA

R. J. SIDDALL
Special Metals Wiggin Ltd., Hereford HR4 9SL, UK

P. D. LEE[†], M. McLEAN
Department of Materials, Imperial College London, SW7 2BP, UK
E-mail: p.d.lee@imperial.ac.uk

The development of grain structure during Vacuum Arc Remelting (VAR) of INCONEL[1] alloy 718, a nickel-based superalloy, is complex depending both on compositional variations and a range of process parameters. A multiscale model is presented which combines a macroscopic solution of the heat transfer, fluid flow and electromagnetism with a mesoscopic model of grain nucleation and growth. The model was used to investigate the influence of variations in process control parameters upon the macroscopic molten pool size and shape, together with the predicted grain structure. Simulations of structures produced for variations in melt rate, arc power and arc focus (both thermal and electrical) were compared with observations from instrumented and characterized plant-trials for steady state melting conditions; good agreement was achieved.
© *2004 Kluwer Academic Publishers*

1. Introduction

The manufacture of aerospace gas-turbine discs from nickel-based superalloys, such as INCONEL alloy 718, involves solidification, hot deformation and heat treatment steps, each of which can influence the final disc homogeneity and microstructure. Vacuum arc remelting (VAR) is the most widely used secondary remelting process for the production of fully dense and homogeneous ingots of reactive and macrosegregation-sensitive alloys. The grain structure of the final wrought disc is dependent upon the initial as-cast ingot grain and segregation structure, together with the recrystallisation occurring during the subsequent deformation processes. The main objective of controlling the VAR process is to produce an ingot with a fine microstructure, no macroscopic segregation and with no unacceptable melt-related such as freckles or white spots.

The grain structure of the VAR ingot is critically dependent upon the temperature distribution and fluid motion within the molten pool, which in turn are determined by the operational process control parameters. The principal process variables include current, melt rate, arc gap, and annular gap. However, the most important process control parameters in VAR are thought to be current and drip short rate. Any fluctuation in these parameters may alter the heat and fluid flow within the molten pool and therefore generate melt-related defects. As an example, transient variations from the nominal melt rate, called melt rate excursions (MRE's), may occur in the industrial VAR process. The magnitude of a MRE can vary from a few percent to hundreds of percents within a few seconds to tens of minutes. MRE's can cause a range of solidification-related defects such as freckles, white spots, and tree rings. Bertram *et al.* recently investigated the effect of transient melt rate on white spot formation during VAR of alloy 718 in an industrial furnace [1]. Starting from nominal steady-state conditions, the melt rate was decreased in steps and then increased again. The ingot was then examined and they concluded that the formation of solidification white spot was activated once the melt rate was low enough, and then deactivated as soon as the melt rate increased to a sufficiently high level again. Changes in the grain structure as a function of melt rate was not reported.

---

*On leave from Isfahan University of Technology, Isfahan, Iran.
[†]Author to whom all correspondence should be addressed.
[1]Trademark of Special Metals Corporation.

Various numerical simulations of the VAR process have been developed over the last twenty years to progressively provide more insight into the relationship between the process parameters and the heat/current/mass transport occurring during VAR. Early VAR models focused on first the macroscopic heat transfer, and then fluid flow for steady state [2–6]. More recent process models have tracked the evolution of the molten pool along the length of the ingot [4]. Empirical equations for predicting the microstructure were then added in the macromodels of secondary processes [7]. Recently, stochastic mesoscopic models have been developed to simulate the dendritic grain structure in secondary remelting processes [8–10]. These mesoscopic models allowed the possible mechanisms for the formation of tree-ring during the VAR of alloy 718 to be modeled, determining the conditions under which tree-rings form [11].

In this article, grain structure formation has been modeled using a multiscale VAR model. The effects of varying the process parameters of melt rate, arc power and arc focus (both thermal and electrical) were studied.

2. Model theory
2.1. Macromodel
The macroscopic modeling of heat transfer, fluid flow, solidification and electromagnetics was performed using the VAR model developed by the Specialty Metals Processing Consortium (SMPC). The model, which is based on the finite difference (FD) method, has been described in detail in a prior publication [6]. The present study desired to explore how changes in the input arc configuration and amount of arc heating could affect the final ingot structure. The model parameters that describe the arc configuration and heating are the thermal focus, the electrical focus, the fraction of current passing between the electrode and ingot, and the amount of thermal heat in the arc that goes to the top of the molten pool. The current, and hence arc heat, that does not enter the ingot is assumed to pass through the arc plasma directly between the ingot and the crucible side wall above the ingot surface. Two other important parameters are the thermal expansion coefficient and a turbulence multiplier factor; both alter the balance of Lorentz to buoyancy forces and hence strongly affect the fluid flow. These model parameters were adjusted within physically realistic ranges to establish a base case solution until the molten pool and thermal environment were found to reasonably approximate the pool depth and solidification environment of a production ingot observed experimentally for comparison to this study.

The variations in arc focus and arc heating studied were based on how the model handles and distributes the above parameters. The model automatically balances the input power to several sources of energy dissipation. Input power is defined as the power supply current multiplied by the machine voltage measured at the bus bars; $P_{\text{total}} = I_{\text{b}} * V_{\text{b}}$. This total power is considered to be the sum of the power required to raise the

metal to its superheat temperature, the thermal energy lost directly to the crucible wall and the thermal energy transmitted to the top surface of the pool by the arc. The first term is related to the steady state melt rate of the process. The second term depends on the fraction of the input current that passes directly from crucible or crown to the electrode generating anodic surface heating at the crucible wall. The third and remaining term is taken as the difference between the total power input and the other two terms. It is the thermal energy imparted to the pool again by anodic surface heating. In equation form [6, 12, 13]:

$$P_{\text{arc}} = I_{\text{b}} * V_{\text{b}} - (\text{d}m/\text{d}t) * h_{\text{sup}} - (1 - C_{\text{b}}) * I_{\text{b}} * V_{\text{e}}, \quad (1)$$

where, P_{arc} is the arc thermal power, I_{b} the bus bar current, V_{b} the bus bar voltage, $\text{d}m/\text{d}t$ the melt rate, h_{sup} the enthalpy to superheat temperature, C_{b} the fraction of bus bar current entering the pool surface, and V_{e} the average anodic surface voltage drop ($V_{\text{e}} \cong \frac{1}{2} V_{\text{b}}$). In this study we elected to change the arc power by simply changing the bus bar voltage. This increases P_{total} and P_{arc} while holding the other terms constant. When simulating melt rate changes, the bus bar current and voltage were changed to match the values expected in real melts, while the arc focus was kept constant.

The distribution of the arc current and the thermal energy on the pool top are each represented by separate Gaussian distributions, which are specified by entering a characteristic 'radius' into the model parameter table. Reducing the radius 'focuses' either the current or thermal input more towards the centre of the pool.

TABLE I Simulation parameters used in the multiscale VAR model

Property	Value	Units
FD macromodel		
Ingot radius	0.255	m
Ingot height (to reach steady state)	1.02	m
Electrode radius	0.217	m
Power	144.9	kW
Efficiency of power	45.0	%
Current	6.3	kA
Volts	23	V
Electrical arc focus	0.17	m
Thermal arc focus	0.35	m
Melt rate	6.47×10^{-2}	kg/s
Casting speed	4.23×10^{-5}	m/s
Turbulence factor	60	%
Gap formation temperature	1503	K
Temperature of mould wall	400	K
Cell size	8.5×10^{-3}	m
Heat transfer coefficient estimates at the ingot/crucible interface		

T (K)	500	750	1000	1250	1400	1485	>1570
h_{c} (W/m²K)	20	34	57	107	192	317	70

CA mesomodel		
Nucleation curve centroid	18.0	K
Nucleation curve distribution	1.5	K
Maximum grain density	$2 \times 10^{+9}$	1/m³
Growth coefficient	1×10^{-7}	m/s/K
Cell size	5.1×10^{-4}	m
Time step	5	s

TABLE II Thermophysical properties of INCONEL alloy 718 nickel-based superalloy

Property	Value	Units
Density	7491	Kg/m^3
Liquidus temperature	1609	K
Solidus temperature	1533	K
Thermal expansion coefficient	1.2×10^{-5}	1/K
Latent heat	2.72×10^5	J/kg
Specific heat	620	J/kg·K
Thermal conductivity	25	W/m·K
Viscosity	5.0×10^{-3}	Pa·s
Electric conductivity	1.0×10^6	1/Ω m
Magnetic permeability	1.26×10^{-6}	H/m

Thus, the arc 'focus' was changed by either increasing or decreasing the radii around a central value.

2.2. Mesomodel

Grain structure formation during the VAR process was modeled using a Cellular Automaton (CA) model. Full details of the microstructural model are given elsewhere [9, 14]. The model is briefly summarized here for completeness. The computation domain is divided into a regular array of square cells whose size is in the range of the microstructural features. A stochastic nucleation model in which a random selection of nuclei each having its own critical undercooling distributed within the domain simulates the nucleation of grains. A distribution of pre-existing nuclei was also located at the external boundary of the domain, representing the chill zone next to the water-cooled crucible.

The solidifying cells grow at a rate, v, determined by the tip undercooling, ΔT_t, which is calculated via a power function as predicted by Kurz *et al.* [15]:

$$v = a_2(\Delta T_t)^2 + a_3(\Delta T_t)^3, \qquad (2)$$

where a_2 and a_3 are growth constant coefficients. The growth rate determines the positions of the corners of an imaginary square, whose crystallographic orientation and centre represent the orientation and preferred growth direction of the grain via a decentered square algorithm. This allows a population of grains to be simulated, each grain having its own preferred growth direction. When the half size of the growing square is large enough to touch any of its neighboring cells, the neighboring cell will be captured (further details given in [14]).

2.3. Multiscale link

The temperature field predicted by the FD macromodel was put into the CA mesomodel using a linear interpolation between the macromodel time steps. As the CA domain is static while the FD domain is growing during the process, any part of the whole calculation domain (CA domain) located above the FD mesh was assigned the maximum temperature found in the FD mesh, and any part located below the FD mesh was assigned the minimum.

3. Results & discussion
3.1. Base case model conditions

The macromodel used has been tested against several industrial conditions [6], however, many of the boundary conditions (BC's) and alloy properties can not be
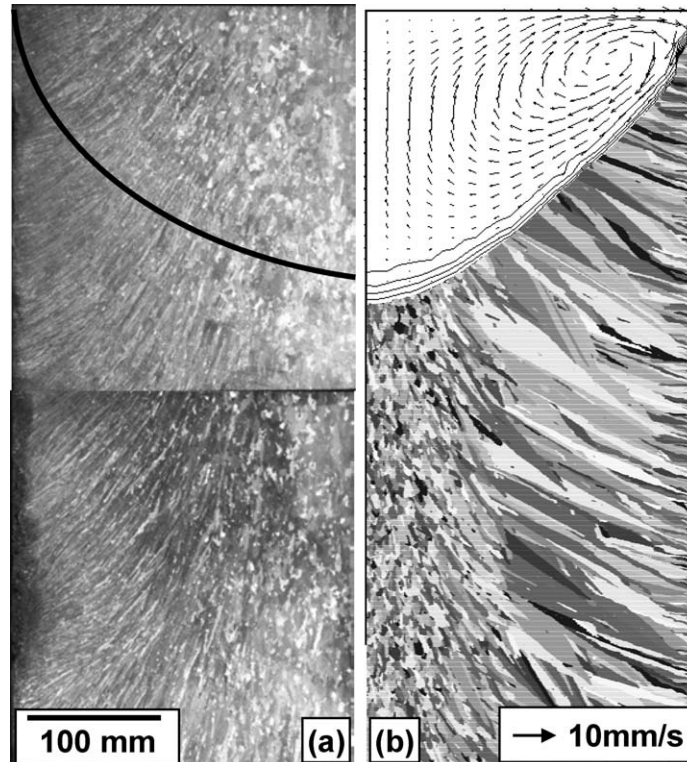

Figure 1 Comparison of (a) the experimental macrostructure with (b) the grain structure predicted by the multiscale VAR model. The solid line delineates the experimentally measured pool shape in (a), while the lighter lines in (b) mark isotherm starting at the liquidus temperature and every 2°C down. The small arrow in (b) shows the vector length in the flow pattern.
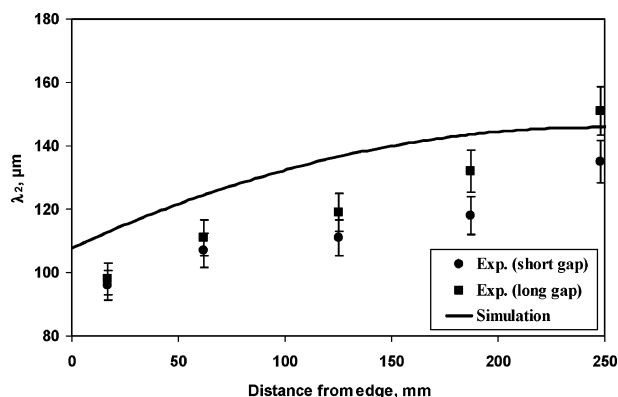
Figure 2 Secondary dendrite arm spacing as a function of distance from edge of the alloy 718 VAR ingot.

TABLE III Nominal parameter values together with the range of variation in the sensitivity study

Parameter	Initial value	Changed value	% Change	Comment
Melt rate (g/s)	64.7	80.1	+25	Via changing the
		48.5	−25	arc current and
				arc voltage
Arc voltage (V)	23	25	+9	Arc power +25%
		27	+17	Arc power +50%
		28.8	+25	Arc power +75%
		21	−9	Arc power −25%
		19	−17	Arc power −50%
		13.8	−25	Arc power −75%
Arc focus	170, 350	350, 350	+100	Diffuse arc
(electrical,		100, 350	−40	Constricted arc
thermal) (mm)		350, 700	+100	Diffuse arc
		100, 200	−40	Constricted arc

easily measured, and hence a study of the influence of these parameters on the model predictions was undertaken. To provide data to establish the base conditions and for validation, an instrumented VAR ingot of alloy 718 superalloy of 510 mm diameter was produced at Special Metals Wiggin Ltd. using nominal processing conditions. The ingot was then sectioned and polished to determine both pool shape and grain structure, as detailed by Xu *et al*. [16]. This VAR process was then simulated with the multiscale model using the simulation parameters and the thermophysical properties listed in Tables I and II.

The model parameters that were not well known and were selected to set up a base case included: (i) thermal focus; (ii) electrical focus; (iii) thermal expansion coefficient; and (iv) the turbulence multiplier factor (used to account for the effects of turbulence in the molten

pool [6]). The value of these parameters was decided by comparison to experimental observations of: (i) molten pool depth and shape; and (ii) secondary dendrite arm spacing. Each of the parameters was altered over a range of values and the following conclusions were reached:

- Increasing the electrical Gaussian radius (decreasing electrical focus) reduces the depth of the molten pool and thickens the mushy zone due to the weakening of the Lorentz flow cell, allowing the buoyancy flow cell to dominate. Altering the thermal Gaussian radius (decreasing thermal focus) has the opposite effect, although the changes were minor over the range of electrical radii studied.
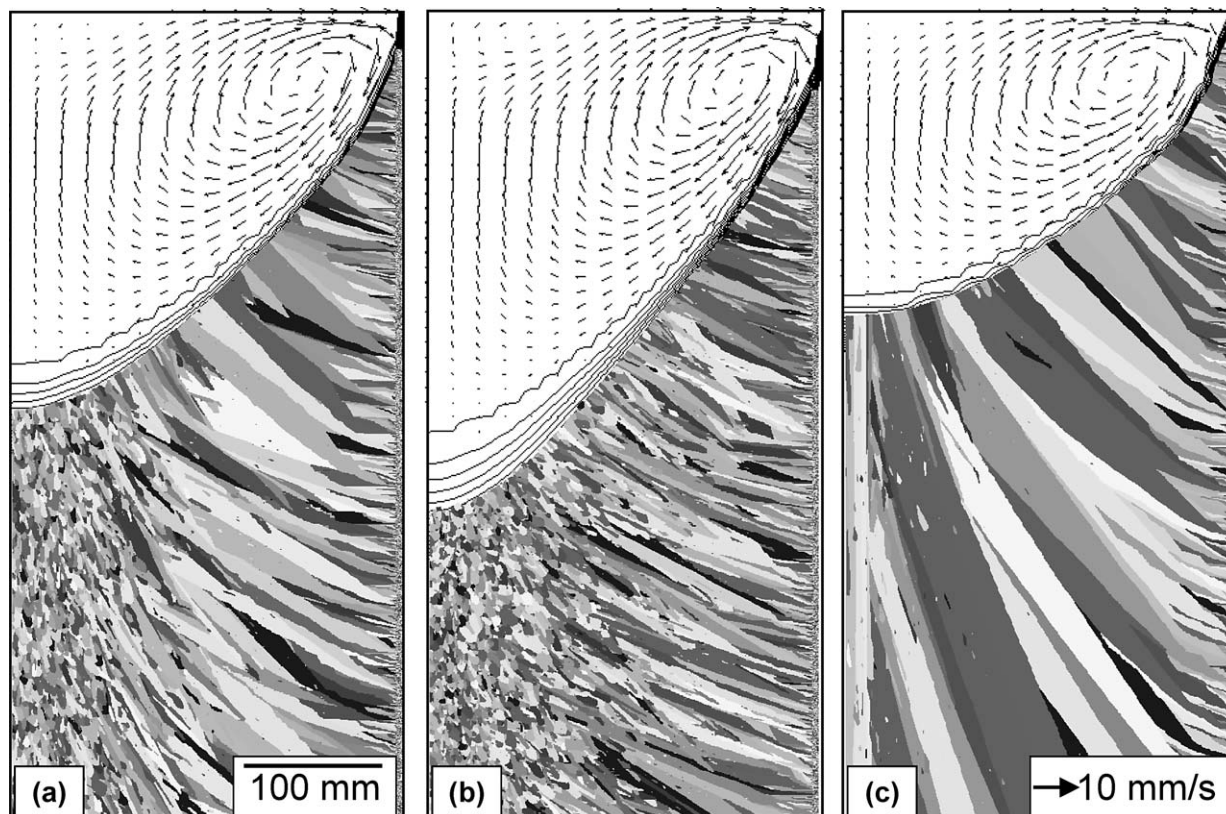

Figure 3 Effect of melt rate on the grain structure of the alloy 718 VAR ingot: (a) 64.7 g/s (the base case); (b) 80.1 g/s (+25%); (c) 48.5 g/s (−25%). The lines mark isotherms starting at the liquidus temperature and every 2°C down.
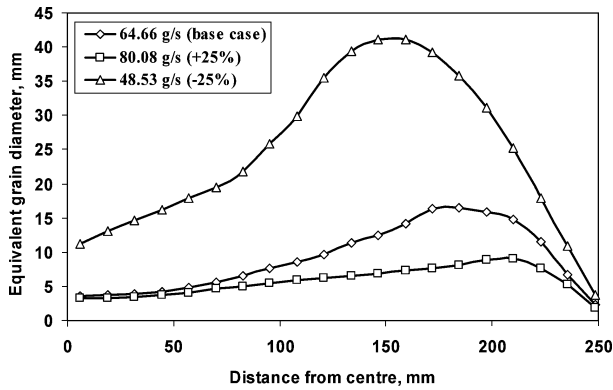
Figure 4 Radial distribution of grain size for different melt rates.

- Increasing thermal expansion coefficient of the melt reduces the depth of the molten pool and thickens the mushy zone since it strengthens the buoyancy cell.
- Increasing the turbulence factor deepens the molten pool and reduces the mushy zone thickness.

By analyzing the above trends, the values of the base case parameters were selected and the multiscale model was used to predict both the macroscopic and microscopic features which are compared to the experimental observations in Fig. 1. The molten pool shape calculated by the interpolation of the tree rings is shown as a black line in the optical macrograph [17]. A reasonable qualitative agreement can be seen between the model simulation and experimental results for both pool shape and the more sensitive grain structure. The maximum fluid velocity seen in the simulations was of the

order of 10 mm/s. The lower temperature gradient in the centre of the pool compared to the mid-radius facilitates grain nucleation and results in a central equiaxed structure.

Another feature for comparison is the secondary dendrite arm spacing, which can be determined from the model via the local solidification time (i.e., or the thickness of the mushy zone when the melt rate is constant) [18]. The calculated secondary dendrite arm spacing is compared with the experimental measurements in Fig. 2, showing a qualitative agreement. With the agreement achieved, the values of the boundary conditions and properties used to generate Fig. 1 (listed in Tables I and II) were therefore used as the base case conditions.

3.2. Sensitivity of grain structure to process parameters
The process parameters studied in this work include melt rate, arc power and arc focus. Their nominal values and the range of variations are listed in Table III. The range of variations for the process parameters considered approximate the fluctuations which might occur in industrial trials. Only the variations over long periods of time were studied, rather than instantaneous or short duration changes.

3.2.1. Effect of melt rate
Melt rate, the mass transferred from the electrode to the ingot per unit time, is one of the most important parameters in industrial practice. Changing the melt rate
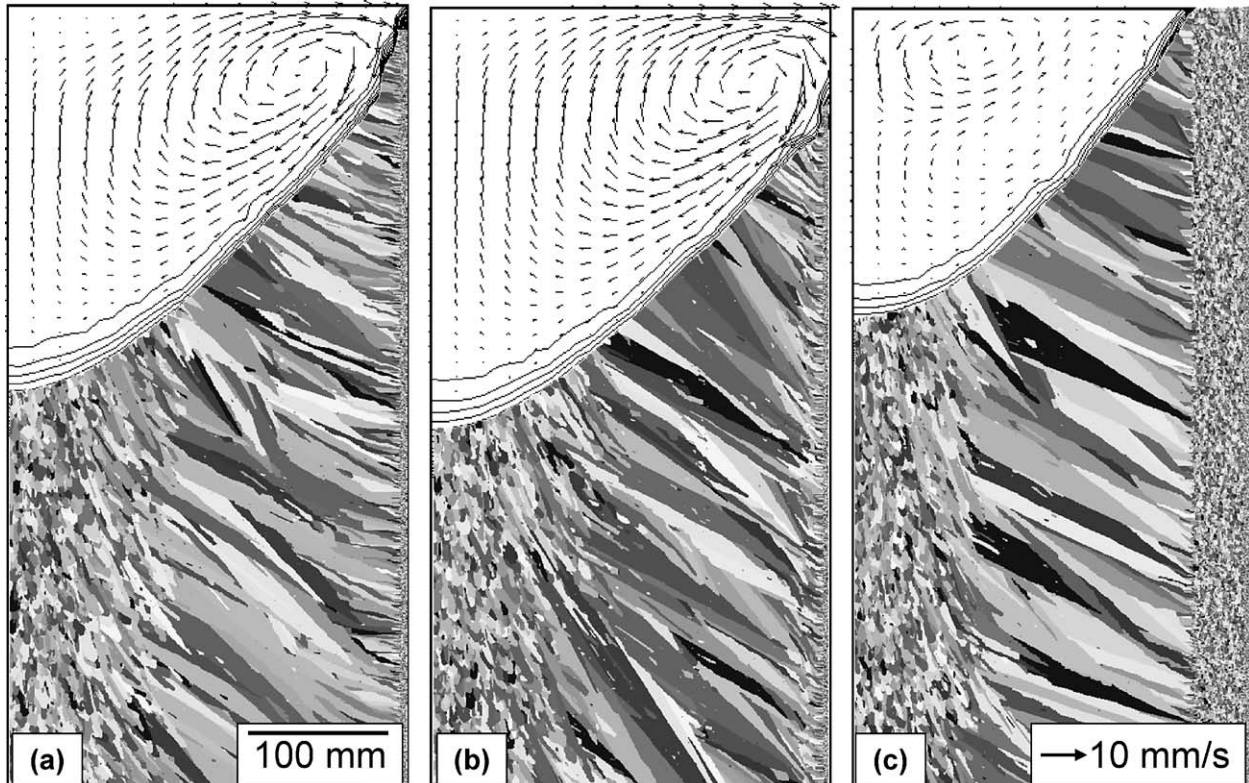

Figure 5 Effect of arc voltage (power) on the grain structure of the alloy 718 VAR ingot: (a) 23 V (the base case); (b) 29 V (75% power increase); and (c) 14 V (75% power decrease). The lines mark isotherms starting at the liquidus temperature and every 2°C down. (Note that in (c) the edge of the ingot is never molten in the macromodel, hence the grain structure predicted is not valid.)
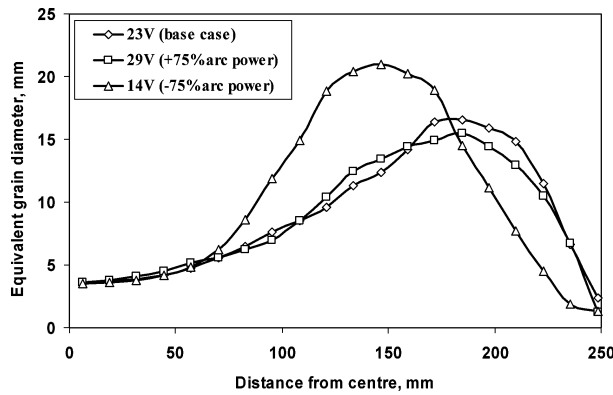
Figure 6 Radial distribution of grain size for different arc voltages.

affects the grain structure of the VAR ingot [11] as well as the shape and depth of the melt pool, influencing the formation of freckles and white spots [19]. In order to study the effect of melt rate on grain structure, arc current and voltage were adjusted so that the expected extent of the melt rate was achieved. No attempt was made to change arc focus, though one might expect the arc to be somewhat more focused at higher currents. Different simulations were carried out from the cold start. Fig. 3 shows the predicted grain structures for the different melt rates. Increasing the melt rate increases the heat input, deepens the molten pool and extends the mushy zone. This not only decreases the temperature gradient (see the wider mushy zone in Fig. 3b) and facilitates nucleation, but also due to extension of the mushy zone makes it more probable that new nuclei will form far away enough from the

solidification front so that they can appear as equiaxed grains blocking the columnar grains. On the other hand, decreasing the melt rate reduces the pool depth as well as the mushy zone size. Under the higher temperature gradient in this condition (see the narrower mushy zone in Fig. 3c) no nuclei can be produced. This significantly affects grain structure formation causing a completely columnar structure with only a 25% decrease in melt rate. The radial distribution of average grain size values predicted by the multiscale model is shown in Fig. 4 for different melt rates. The grain size data plotted are weighted average values. As can be seen, while decreasing melt rate significantly increases the average grain size, increasing melt rate causes a finer and more uniform grain structure.

3.2.2. Effect of arc power

The arc power supply was defined in the model as the heat transferred from the electrode to the ingot excluding both the enthalpy transferred by the molten drops as well as the power lost through the sidewalls. In this analysis, the arc power was changed by altering the bus bar arc voltage rather than the current in order to keep other parameters constant. Changing the arc voltage (power) alters the pool depth and the competition between the buoyancy and Lorentz flow cells. Different simulations were carried out for different arc voltages from the cold start. Fig. 5 compares some of the grain structures predicted in the ingot for the arc voltages considered. Increasing the arc voltage deepens the melt pool and increases the temperature gradient in the top surface of the melt; however, it doesn't seem to have
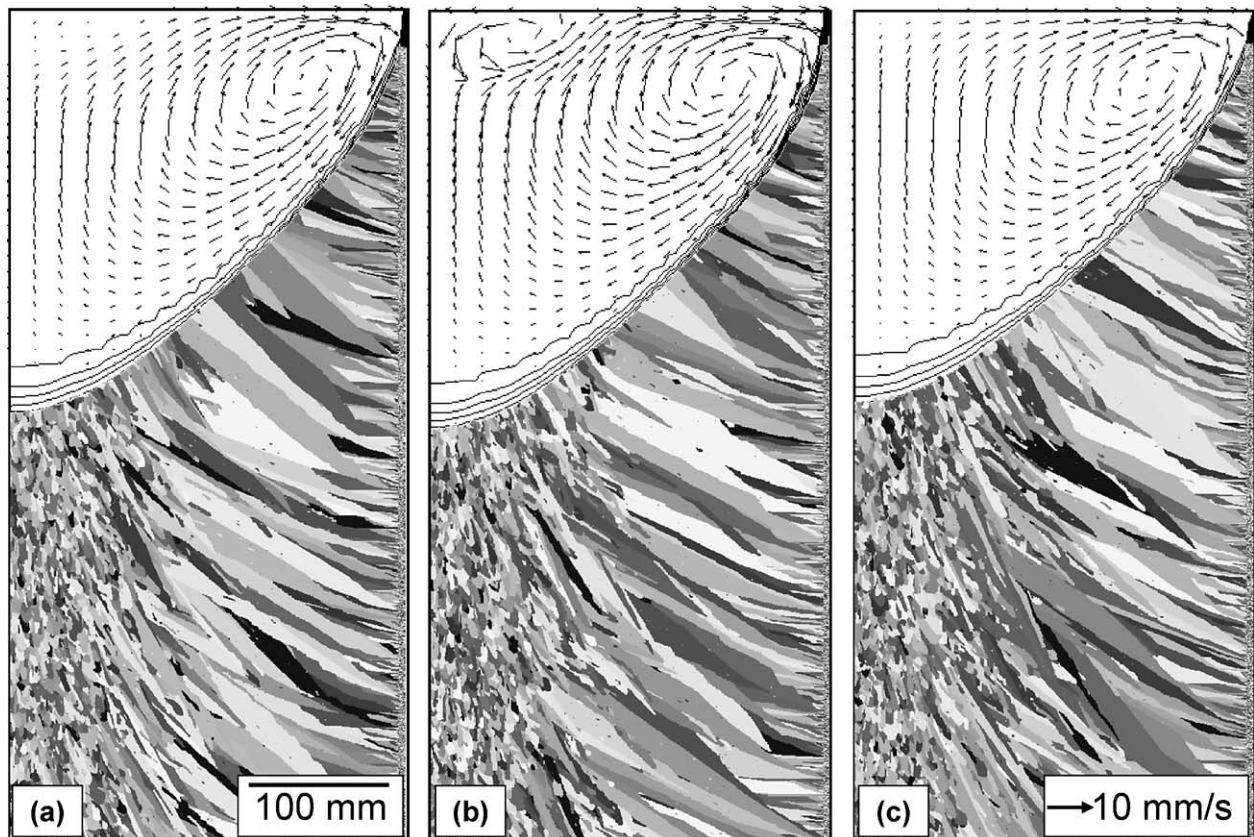

Figure 7 Effect of arc focus (electrical & thermal) on the grain structure of the alloy 718 VAR ingot: (a) 170 & 350 mm (the base case); (b) 100 & 200 mm; and (c) 350 & 700 mm. The lines mark isotherms starting at the liquidus temperature and every 2°C down.
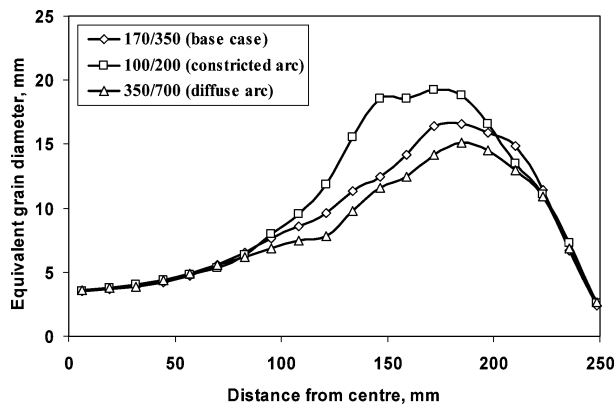
Figure 8 Radial distribution of grain size for different arc focuses (electrical/thermal radii in mm).

a big influence on the overall ingot grain structure. On the other hand, reducing the arc voltage decreases the pool depth and weakens the buoyancy cell. As a consequence, the amount of the hot metal transferring from the pool centre beneath the arc towards the edge will be decreased. Moreover, the stronger Lorentz cell pushes more hot metal down along the centre line causing a higher temperature gradient in the centre and smaller central equiaxed zone. The radial distribution of the average grain size is shown in Fig. 6. The average grain size values for the higher voltage is almost in the range of the base case, but is clearly different from the lower voltage.

3.2.3. Effect of arc focus

The radius of the Gaussian distribution function (the inverse of the arc focus) was changed for both thermal and electrical fluxes to investigate their influence on grain structure. In this study, different simulations were carried out for different arc focuses from the cold start. Fig. 7 compares the predicted grain structure for the base case (with 170 mm electrical and 350 mm thermal arc radii) with more constricted and diffuse arc focuses. Increasing the arc focus (decreasing the Gaussian radius) deepens the pool and strengthens the Lorentz cell. This introduces more heat into the centre of the pool, decreasing the tip undercooling within the mushy zone, resulting in less nucleation. On the other hand, decreasing the arc focus (increasing the Gaussian radius) does not significantly affect the heat transfer condition in the pool and therefore the overall grain structure. The radial distribution of average grain size values is shown in Fig. 8. The grain size distribution for the diffuse arc (with 350 mm electrical and 700 mm thermal arc radii) is almost the same as the base case; however, the constricted arc (with 100 mm electrical and 200 mm thermal arc radii) shows a narrower central equiaxed zone along with coarser columnar grains.

4. Conclusions

A multiscale numerical VAR model was developed to investigate the effect of variations in process control parameters upon both the macroscopic molten pool shape/depth and the predicted grain structure. Variations in melt rate, arc power and arc focus were

compared to instrumented and characterized plant-trials for the steady state condition. It was found that while increasing the melt rate by 25% expands the central equiaxed region and refines the columnar grains, reducing the melt rate by the same proportion produces a completely columnar grain structure. Although increasing the arc voltage by 25% (equivalent to increasing power by 75%) does not show a significant effect on the grain structure, reducing the arc voltage by the same proportion significantly extends the chill zone and shrinks the central equiaxed region. A diffuse arc (increasing the radius by 100%) does not change the overall grain structure; however, a constricted arc (decreasing by 40%) slightly reduces the central equiaxed zone and coarsens the columnar grains.

References
1. L. A. BERTRAM, J. A. BROOKS, D. G. EVANS, A. D. PATEL, J. A. VAN DEN AVYLE and D. D. WEGMAN, in Proceedings of the Int. Symp. on Liq. Met. Proc. and Cast., Santa Fe, New Mexico, USA, Feb. 21–24, 1999, edited by A. Mitchell *et al*. (AVS, 1999) p. 156.
2. A. S. BALLANTYNE and A. MITCHELL, *Ironmak. Steelmak.* **4** (1977) 222.
3. L. A. BERTRAM and F. J. ZANNER, in Proceedings of the Metal. Appl. of Magnetohyd., Cambridge, UK, edited by H. K. Moffatt and M. R. E. Proctor (TMS, 1982) p. 283.
4. A. JARDY, L. FALK and D. ABLITZER, *Ironmak. Steelmak.* **19** (1992) 226.
5. A. JARDY and D. ABLITZER, in Proceedings of the Mod. Cast. Weld. Adv. Solid. Proc. V, Davos, Switzerland, edited by M. Rappaz *et al*. (TMS, 1990) p. 699.
6. L. A. BERTRAM, C. B. ADASCZIK, D. G. EVANS, R. S. MINISANDRAM, P. A. SACKINGER, D. D. WEGMAN and R. L. WILLIAMSON, in Proceedings of the Int. Symp. on Liq. Met. Proc. and Cast., Santa Fe, New Mexico, USA, edited by A. Mitchell and P. Auburtin (AVS, 1997) p. 110.
7. P. D. LEE, R. LOTHIAN, L. J. HOBBS and M. MCLEAN, in Proceedings of the Superalloys 1996, Warrendale, PA, edited by R. D. Kissinger *et al*. (TMS, 1996) p. 435.
8. L. NASTAC, S. SUNDARRAJ, K. YU and Y. PANG, in Proceedings of the Int. Symp. on Liq. Met. Proc. and Cast., Santa Fe, New Mexico, Feb. 16–19, 1997, edited by A. Mitchell and P. Auburtin (AVS, 1997) p. 145.
9. X. XU, R. C. ATWOOD, S. SRIDHAR, P. D. LEE, M. MCLEAN, B. DRUMMINGS, R. M. WARD and M. H. JACOBS, in Proceedings of the Int. Symp. on Liq. Met. Proc. and Cast., Santa Fe, New Mexico, USA, edited by A. Mitchell *et al*. (AVS, 1999) p. 76.
10. L. NASTAC, *Int. J. Cast Metals Res.* **15** (2002) 279.
11. X. XU, W. ZHANG and P. D. LEE, *Metal. Mater. Trans.* A **33A** (2002) 1805.
12. D. G. EVANS and R. ERDMANN, Personal Communication, Special Metals Corporation, New Hartford, NY, 2003.
13. K. O. YU, in Proceedings of the Specialty Metals Melting and Processing, Pittsburg, Pensylvania, 11–13 June, 1984, edited by 1984.

14. W. WANG, A. KERMANPUR, P. D. LEE, M. MCLEAN, X. WANG, R. M. WARD and M. H. JACOBS, in Proceedings of the Int. Symp. on Liq. Metal Proc. and Cast., Santa Fe, New Mexico, Sept. 23–26, 2001, edited by A. Mitchell and J. Van Den Avyle (AVS, 2001) p. 267.

15. W. KURZ, B. GIOVANOLA and R. TRIVEDI, *Acta Metal.* **34** (1986) 823.

16. X. XU, R. M. WARD, M. H. JACOBS, P. D. LEE and M. MCLEAN, *Metal. Mater. Trans.* A **33** (2002) 1795.

17. R. M. WARD, T. P. JONHSON and M. H. JACOBS, in Proceedings of the Int. Symp. on Liq. Met. Proc. and Cast., Santa Fe, New Mexico, USA, edited by A. Mitchell and P. Auburtin (AVS, 1997) p. 97.

18. P. D. LEE, P. N. QUESTED and M. MCLEAN, *Phil. Trans. R. Soc. Lond.* A **356** (1998) 1027.

19. A. D. HELMS and C. M. O'BRIEN, *JOM* **50** (1998) 12.